

A New Label-Free Approach to Glioblastoma Cancer Stem Cell sorting and detection.

Aurélie Lacroix^{1*}, Elise Deluche^{1,2*}, Ling Yan Zhang³, Claire Dalmay³, Carole Mélin¹,
Jonathan Leroy³, Meissa Babay³, Christophe Morand Du Puch⁴, Stéphanie Giraud⁴, Barbara
Bessette¹, Gaëlle Bégaud¹, Sofiane Saada¹, Christophe Lautrette⁴, Arnaud Pothier³, Serge
Battu^{1*}, Fabrice Lalloué^{1*}

1. EA3842- CAPTuR, GEIST, Université de Limoges, Limoges, France. Faculté de Médecine, 2 rue du Dr Marcland, 87025 Limoges Cedex
2. Department of Medical Oncology, Limoges University Hospital, 2 rue Martin Luther King, 87042 Limoges, France
3. XLIM-UMR CNRS 7252, Université de Limoges, Limoges, France, 123, avenue Albert Thomas - 87060 LIMOGES CEDEX.
4. Oncomedics, Ester Technopole, Limoges, France

* Equal contribution

✉ Corresponding author: serge.battu@unilim.fr

Abstract

Cancer stem cells (CSCs) play critical roles in cancer, making them important targets for new diagnostic and therapeutic approaches. Since CSCs are heterogeneous and not abundant in tumors, and few specific markers for these cells currently exist, new methods to isolate and characterize them are required. To address this issue, we developed a new label-free methodology to isolate, enrich, and identify CSCs from an heterogeneous tumor cell subpopulation using a cell sorting method (Sedimentation Field Flow Fractionation, SdFFF) and a biosensor as a detector. Enrichment was optimized using an original protocol and U87-MG glioblastoma cells cultured in Normal (N) or Defined (D) medium (\pm Fetal Bovine Serum, FBS) under Normoxic (N, $pO_2 = 20\%$) or Hypoxic (H, $pO_2 < 2\%$) conditions to obtain four cell populations: NN, NH, DN, and DH. After elution of CSCs via SdFFF using the hyperlayer mode (inertial elution mode for micron-sized species), we isolated eight subpopulations with distinct CSC contents based on phenotypical and functional properties, ranging from NN F1 with a lower CSC content to DH F3 with a higher CSC content. Reflecting biological differences, the intrinsic intracellular dielectric permittivity increased from NN to DH conditions. The largest difference in electromagnetic signature was observed between NN F1 and DH F3, in which the CSC content was lowest and highest, respectively. The results demonstrate that microwave dielectric spectroscopy can be used to reliably and efficiently distinguish stem cell characteristics. This new instrumental and methodological approach is an important innovation that allows both enrichment and detection of CSCs, opening the door to novel diagnostic and therapeutic approaches.

Key words: Cancer Stem Cells, SdFFF, biosensor, dielectric spectroscopy, electromagnetic signatures

Proof Version

Introduction

Malignant gliomas, including glioblastoma multiforme (GBM; World Health Organization [WHO] grade IV), are among the most lethal malignancies¹. Despite recent advances in surgery, imaging, radiation therapies, and chemotherapy, the prognosis of GBM is still dismal², primarily due to the recurrence of tumors that are resistant to radio- and chemo-therapy treatments³. Accumulating evidence indicates that the hypoxic regions of heterogeneous solid tumors contain a restricted cell population, termed cancer stem cells (CSCs) that promote tumor formation, progression, and relapse⁴⁻⁷. These cells are resistant to ionizing radiation^{8, 9} and chemotherapy¹⁰, are few in number, and are not easily identified and isolated.

CSCs and normal stem cells share some biological features; therefore, the markers of these two cell types are similar. CSCs have been identified in several cancers^{11, 12} using one or more markers, including CD34¹³, CD39¹⁴, CD44¹⁵, CD133^{16, 17}, ALDH1^{18, 19}, and Hoechst exclusion^{11, 20}. However, a single marker is insufficient to isolate CSCs. Thus, controversy surrounds the membrane protein CD133²¹, which was long considered to be a gold standard for identification of CSCs in several types of cancer¹¹. Indeed, expression of CD133 is not restricted to CSCs, which calls into question its use and reliability as a unique CSC marker to characterize these cells^{22, 23}. Therefore, it is currently advised that several CSC markers are combined to improve the characterization of CSCs and to increase the amount and purity of isolated CSCs. Furthermore, functional tests, such as the colony formation assay and tumor xenografts *in vivo*, that assess the specific features of CSCs, such as their self-renewal ability and capacity to regenerate tumors, are also valuable for characterization of CSCs. Unfortunately, phenotypic changes can occur due to the reversible nature of the stemness status, leading to transient loss of CSC markers²⁴. Altogether, these data show that isolation and characterization of CSCs from

heterogeneous cell populations remain difficult and require the development of new label-free methods that can be used in combination with conventional methods to characterize CSCs. New label-free methods might avoid problems associated with the plasticity of CSCs and ensure that CSCs are isolated and characterized with limited cellular changes induced by immunological labeling, which is commonly performed in cell sorting methods. Accordingly, we devised a novel, label-free method that combines two approaches for sorting and characterization of CSCs. The first approach depends on Sedimentation Field Flow Fractionation (SdFFF), which increases the purity of subpopulations with different degrees of differentiation (*e.g.*, differentiated cells *vs.* CSCs). The second approach uses high-frequency dielectric spectroscopy with highly sensitive resonant microwave biosensors, which generate specific electromagnetic (EM) cell signatures that reflect the CSC content.

SdFFF is a gentle, non-invasive, and tagless method that is particularly well suited to sorting stem cells and monitoring biological events. Its advantages are based on its drastic limitation of cell–solid phase interactions through the use of (i) an empty ribbon-like channel without a stationary phase; and (ii) the “hyperlayer” elution mode, a size/density-driven separation mechanism. Cell separation depends on differential elution of species *via* the combined action of a parabolic profile generated by flowing a mobile phase through the channel and a multigravitational external field (generated by rotation of the channel) applied perpendicularly to the flow direction. Over the past decade, applications of SdFFF cell sorting have been developed in many fields, including stem cell biology²⁵, oncology²⁶, and CSC sorting²⁷.

Conventional dielectric spectroscopy uses a narrow band (5–20 GHz), corresponding to microwave region of the EM spectrum, and permits characterization of cell contents and a

means to discriminate and analyze cells. This approach takes advantage of the interaction between high-frequency EM fields and the physical properties of biological cells, *e.g.*, the complex dielectric permittivity of intracellular contents^{28, 29}. Notably in this regard, the permittivity of cell contents depends on frequency^{30, 31}. At low frequencies (up to a few MHz) the lipid bilayer of the cell membrane acts as an electrical insulator, preventing most EM fields from penetrating the cell. At higher frequencies, up to the GHz range, EM waves can pass through the membrane and interact with organelles and intracellular components. At low magnitudes, such waves can dielectrically probe the cytoplasm without causing damage. Indeed, microwave dielectric spectroscopy is sensitive to water concentration, protein concentration, nuclear size, and macromolecular interactions occurring *in cellulo*^{28, 29}. Measurable differences in dielectric permittivity among cells enable discrimination of overall cell content, indicating that the cells under observation have distinct differentiation status.

In this study, we implemented a microwave dielectric spectroscopy technique using microwave resonant micro-devices whose sensing capability allows measurement of the overall dielectric permittivity of individual biological cells. These biosensors are sensitive to a cell's own bio-impedance at high frequencies, especially in the GHz frequency range. The sensing principle is based on detection of a change in the overall capacitance of the sensor when it is loaded with cells: specifically, localization of cells on the sensing area increases sensor capacitance. This change in capacitance alters the biosensor's resonance frequency, and the resultant frequency shift can be directly related to the intrinsic dielectric properties of the cell using appropriate biophysical modeling³².

In our method, we initially grew an U87-MG glioblastoma cell line in various medium (Normal (N) and Defined (D)) under different oxygen conditions (Normoxic (N) and Hypoxic

(H)) to obtain four cell populations: NN, NH, DN, and DH. Based on expression of CSC-specific markers, the enrichment level of CSCs was distinct in these populations, ranging from NN to DH. Thereafter, SdFFF was performed to increase the CSC content and to generate populations with distinct (low and high) CSC contents. This yielded a unique cell matrix of 8 subpopulations, ranging from F1 NN with the lowest CSC content to F3 DH with the highest CSC content.

Next, biosensors were used for the first time in association with SdFFF cell sorting to obtain specific EM signatures. In each comparison (NN *vs.* DH and F1 NN *vs.* F3 DH), the EM signature revealed a correlation between the CSC content and the normalized dielectric permittivity, which enabled unique and specific determinations of CSC abundance.

Many detectors can be on-line hyphenated with FFF methods to detect and characterize sub-micron particles (macromolecules, colloids, nano-particles, etc.) such as MALS, DLS, and ICP-MS³³. However, to the best of our knowledge, there is no label-free detector for cell sorting. In this context, combining biosensors with SdFFF may be an efficient solution for label-free sorting and characterization of cells. The development of a novel technology that combines cell sorting via SdFFF with an EM signature of GBM CSCs will help to establish a bank of signatures that may be useful for determining tumor aggressiveness based on the CSC content.

Materials and Methods

The overall method is summarized in Figure 1.

Cell culture (Figure 1A)

The human glioblastoma cell line U87-MG was purchased from the American Type Culture Collection (ATCC, Manassas, VA, USA) and grown under four conditions: NN (normal medium [with fetal bovine serum: FBS], normoxic), NH (normal medium, hypoxic), DN (defined medium [serum-free], normoxic), and DH (defined medium, hypoxic).

Normal medium was minimum essential medium (MEM) (Gibco Life Science, Gaithersburg, MD, USA) supplemented with 10% FBS (Gibco Life Science), 50 units/mL penicillin, 50 units/mL streptomycin, 2 mM L-glutamine, 1% non-essential amino acids, 2 mM sodium pyruvate, and 1.5 g/L sodium bicarbonate. Cells were cultured at 37°C in a 5% CO₂ incubator with 20% O₂ (NN) or 1% O₂ (NH).

To obtain neurospheres, U87-MG cells were cultivated in defined serum-free medium consisting of DMEM/F12 (Gibco) supplemented with 50 units/mL penicillin, 50 units/mL streptomycin (Gibco), 2.4 g/L sodium bicarbonate, 1 M HEPES (Sigma-Aldrich, Saint-Quentin-Fallavier, France), 1× progesterone (Sigma-Aldrich), 1× putrescine (Sigma-Aldrich), 0.025 g/mL heparin (Sigma-Aldrich), 30% (w/v) glucose (Sigma-Aldrich), 1× B27 growth supplement (Invitrogen, Carlsbad, CA, USA), 20 ng/mL EGF (Sigma-Aldrich), 20 ng/mL basic human FGF (Sigma-Aldrich), and 1× insulin–transferrin–sodium selenite supplement (Roche Diagnostics, Meylan, France). The primary neurospheres were mechanically dissociated, and cells were seeded to form secondary neurospheres, which were used for experimentation. Cells were cultured at 37°C in a 5% CO₂ incubator with 20% O₂ (DN) or 1% O₂ (DH).

Proof Version

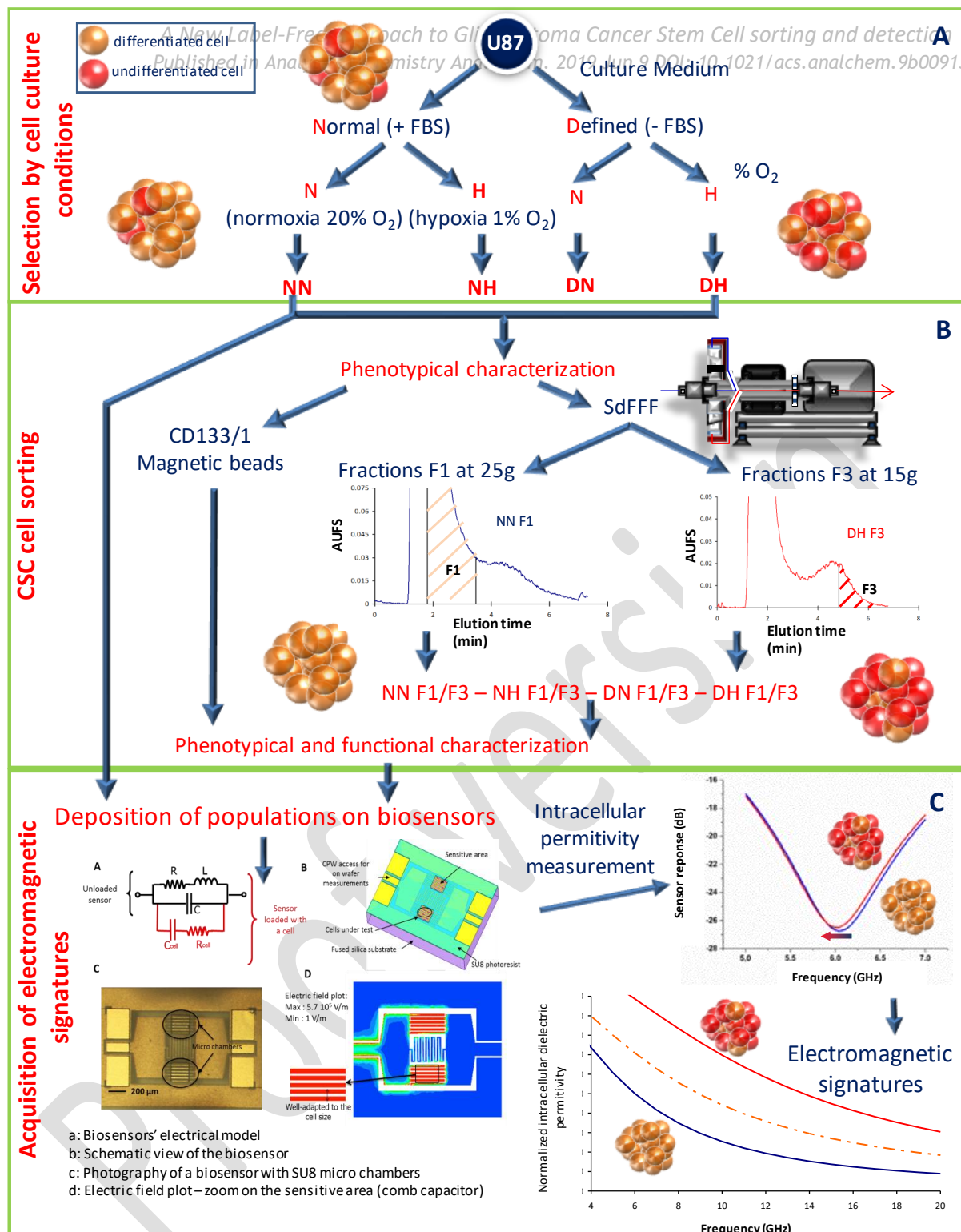


Figure 1. Schematic representation of the overall method. **(A)** Four conditions are established, with differing medium and oxygen conditions (NN, NH, DN, and DH), to obtain various degrees of CSC enrichment. **(B)** CSCs are enriched using the SdFFF cell sorting method, which was compared with the gold standard (classical sorting with CD133/1 magnetic beads). SdFFF was a better cell sorting method than magnetic bead cell sorting. **(C)** SdFFF was then coupled with a series of biosensor analyses, providing specific EM signatures of the eight subpopulations.

Phenotypical and functional characterization of cell subpopulations: see SI-1 and 2

Magnetic CD133/1 beads for cell separation: see SI-3

SdFFF device and cell elution conditions. The SdFFF separation device used in this study was derived from a device that was described and schematized previously³⁴. The apparatus consisted of two $880 \times 47 \times 2 \text{ mm}^3$ polystyrene plates separated by a Mylar[®] spacer into which a channel was carved. The channel had dimensions of $788 \times 12 \times 0.175 \text{ mm}^3$, with two 50 mm V-shaped ends. The measured total void volume (channel volume + connecting tubing + injection/detection device) was $1906 \pm 10.00 \text{ }\mu\text{L}$ ($n = 6$). Void volume was calculated after determination of elution time of a non-retained compound (0.10 g/L benzoic acid, UV detection at 254 nm). The channel rotor axis distance was $r = 14.80 \text{ cm}$. Sedimentation fields were expressed in units of gravity, $1 g = 980 \text{ cm/s}^2$, and calculated as previously described³⁵. Cleaning and decontamination procedures were described previously³⁶. A T90S2 asynchronous motor (Brown Group, Limas, France) was connected to a COMBIVERT F4 pilot unit (Keb, La Queue en Brie, France)³⁷. An LC-20AD UPLC pump (Shimadzu, Champ/Marne, France) was used to pump the sterile mobile phase. Sample injections were performed using a Rheodyne[®] 7125i chromatographic injector (Rheodyne, Cotati, CA, USA). The elution signal was recorded at 254 nm on a SPD-20AV UV/VIS Detector (Shimadzu) with a NI9211 (10 mV input) acquisition device (National Instruments France, Nanterre, France) operated at 3 Hz and connected to a personal computer controlled by Visual Basic software developed in-house (VB pro, Ver 6.0, Microsoft Corp.).

Optimal elution conditions were as follows: flow injection through the accumulation wall of a $100 \text{ }\mu\text{L}$ U87-MG cell suspension ($2 \times 10^6 \text{ cells/mL}$); flow rate: 0.80 mL/min ; mobile phase: sterile PBS, $\text{pH} = 7.4$; and external multigravitational field strength: $15 \text{ or } 25.00 \pm 0.02$

g (312 or 412 ± 0.2 rpm). Time-dependent fractions (F1 and F3) were collected as described in Figure 2B to obtain fractions enriched in differentiated cells or CSCs. To obtain a sufficient quantity of cells for further analysis and subculture, consecutive SdFFF fraction collections were performed³⁶.

EM signature measurements. The biosensors used to investigate EM signatures were designed based on resonance disturbance principles; such sensors have superior sensitivity relative to the broadband characterization techniques conventionally used in microwave spectroscopy³⁸. Specifically, the biosensors were designed with a coplanar topology, using a flattened coaxial waveguide made from thin micromachined metal lines patterned on the same side of a glass substrate. These biosensors operate as bandstop resonators, meaning that they have a specific resonance frequency at which the microwave signal transmitted across the sensor is highly attenuated (Figure 1C). As a result, a peak of microwave power absorption could be observed by measuring the sensor transfer function when the microwave signal frequency was swept continuously through a range.

To design such resonators, a meander line acting as an inductor (L) was connected in parallel with two capacitors with a comb design (i.e., an array of narrow interdigitated electrodes). The geometry of these capacitors is particularly interesting, because in this configuration they strongly concentrate the EM field, especially at the sensor resonance where the electric field is maximal. This results in a highly sensitive detection area that is capable of detecting very small dielectric disturbances on the sensor surface. Hence, the introduction of individual cells between these electrodes, especially in the comb capacitor's gaps, slightly increased the sensor capacitance and thus modified the resonant frequency of the sensor. The induced frequency shift could then be measured, and its value was directly linked to the cell's

own bio-impedance at that specific frequency. Due to their dedicated geometry (i.e., the length and size of the inductor and capacitor), these biosensors achieved high sensitivity, which gave them the capability to operate at very low cell concentrations (down to single cells).

The sensor resonant frequency (F_0 without cells; F_1 once loaded with cells) is determined by equation (1), and depends on the sensor inductance (L , in Henry), the sensor capacitance (C_0 , in Farad), and the additional effect of the cell (C_{cell} , in Farad). As illustrated in Figure 1C, C_0 and C_{cell} respectively model the intrinsic capacitance value of the unloaded sensor (i.e., without cells) and the additional capacitance introduced by cells.

$$F_0 = \frac{1}{2\pi\sqrt{L.C_0}} \quad F_1 = \frac{1}{2\pi\sqrt{L.(C_0 + C_{\text{cell}})}} \quad (1)$$

Because comb capacitors were the most suitable sensor design for characterization of the dielectric properties of cells, it was important to favor optimal localization of cells in the electrode array's gaps. Therefore, specific micro-chambers were patterned using UV photolithography techniques and a 40 μm thick biocompatible photosensitive resist (SU8, MicroChem Corp. Flanders Road Westborough, MA, US). The same micro-chambers were implemented in 10 different sensor designs that were used for this work. Each of them operated at a different resonant frequency from the others, allowing characterization of a cell population on a wider frequency band (here, ranging from 6.2 to 18.1 GHz) than a single resonant sensor, which would only give access to the dielectric properties of cells at its specific resonant frequency. Each of these biosensors had the same capacitance value, C_0 , which was set to ensure the optimal sensitivity of the biosensor. Consequently, the resonant frequency of the various sensors had to be adjusted by tuning the lengths of their inductors (i.e., meander lines) (Figure 5A).

During the experiments, the maximum resonator sensitivity could be reached only if the cells were characterized in air, i.e., outside of their culture media. Conventional biological media are aqueous saline solutions that absorb signal strongly in the microwave frequency range, and consequently degrade the biosensor's detection capability and efficiency.

As a result, cells had to be prepared for measurement in air conditions while maintaining their intracellular content for proper analysis. Therefore, before microwave dielectric spectroscopy, cells were fixed in 4% formaldehyde, rinsed three times in deionized water, and finally resuspended in deionized water. This formed a cell suspension that could be deposited on two sensors used in each experiment. For each sensor, a very small droplet of this suspension (typically hundreds of nL) was injected inside the micro-chambers via a glass capillary connected to a syringe pump. After a few seconds, once the surrounding medium had fully evaporated, the sensors were individually measured. This approach benefited from the evaporation process, which caused the cells to naturally drop down onto the comb capacitor of the resonating sensor, preferentially inserting into the electrode gaps, where they had the maximal influence on the biosensor response.

Sensor RF measurements were performed using a probe station (Süss MicroTEc SE, Schleissheimer, Garching, Germany) dedicated to such experiments; the station was mounted with Ground Signal Ground RF probes (Cascade ACP type) and connected to a vector network analyzer (R&S ZVA-24). This setup allowed recording of each sensor's transfer function via measurement of their scattering parameters (S-parameters) in the targeted frequency band (5–20 GHz). In practice, each sensor was characterized before and after deposition of the cell suspension, strictly following the same procedure and RF setup configuration to ensure proper sensor calibration. As an example, Figure 1C shows a comparison of a biosensor's response

with and without cells. This allowed measurement of the resonant frequency F_0 of the unloaded sensor and F_1 of the loaded sensor with a controlled number of cells under the microscope. Using an analytical model, the dielectric properties of the cells were then extracted from the measured sensor frequency shift $\Delta F = F_1 - F_0$, taking into account the number and size of cells present on both capacitors of the resonating sensor. This model, detailed in³⁸, was developed to compute the real part of the intracellular cell permittivity at the resonant frequency of each sensor. Ultimately, the compilation of all data acquired at the various frequencies enabled establishment of a given EM signature for each cell population. This EM signature is set using model parameters based on an iterative fitting procedure. Hence, to model the reliance of the measured intracellular cell permittivity on the investigated frequency, a commonly used Cole-Cole equation³⁸ has been considered. Only the real part of complex dielectric permittivity was of interest in this study; therefore, the Cole-Cole model was simplified³⁸ in (2).

$$\epsilon_{r_Cell}(\omega) = \frac{\Delta\epsilon_r (1 + (\omega\tau)^{1-\alpha} \sin(\alpha\pi/2))}{1 + 2(\omega\tau)^{1-\alpha} \sin(\alpha\pi/2) + (\omega\tau)^{2-\alpha}} + \epsilon_{r,\infty} \quad (2)$$

where ω is the angular frequency (*i.e.*, $\omega = 2\pi f$) and $\epsilon_{r,\infty}$, $\Delta\epsilon_r$, τ , and α are variable parameters chosen to fit the experimental data.

Statistical analysis

Statistical analyses were performed on three independent experiments using StatView. ANOVA tests were conducted to compare different conditions. Box plots were achieved to enforce SdFFF sorting method choice. P values ≤ 0.05 were considered statistically significant.

Results and Discussion

CSCs are not abundant in tumors or cell lines^{8, 39}, and few markers are available to isolate and characterize these cells in an efficient and specific manner^{11, 12}. The method described in this publication was designed to overcome these challenges. To this end, we established a totally label-free approach by optimizing culture conditions, SdFFF cell sorting, and biosensor characterization (Figure 1).

Production of cell subpopulations with increasing degrees of stemness. Culture of the U87-MG human glioblastoma cell line in different conditions, including culture in different types of medium and/or under different concentrations of oxygen, should allow us to obtain distinct subpopulations (NN, NH, DN, and DH) with varying degrees of stemness (Figure 1A and 2A). CSCs were identified by western blot analysis of conventional markers, including glycosylated CD133/1 and 2, OCT-4, and A2B5 (Figure 2A). Protein expression of CD133/1 and OCT-4, which are highly expressed in CSCs⁴, is particularly important. The marker levels increased progressively according to the culture conditions, from NN to DH in the order NN < NH < DN < D (Figure 2A). Levels of all markers were significantly higher in DH than in NN ($p < 0.001$). This increase was about 1.4-fold for CD133/2, 2.8-fold for CD133/1, 3.1-fold for OCT-4, and 7.2-fold for A2B5. No significant differences for any marker were observed between NN, NH, and DN.

Taken together, these results demonstrate that the combination of defined medium and hypoxia was the most favorable condition for increasing the CSC subpopulation. Indeed, DH conditions promoted expression of CD133/1, OCT-4, and A2B5. Based on the reliability of these markers, we used them in further experiments to accurately discriminate CSCs.

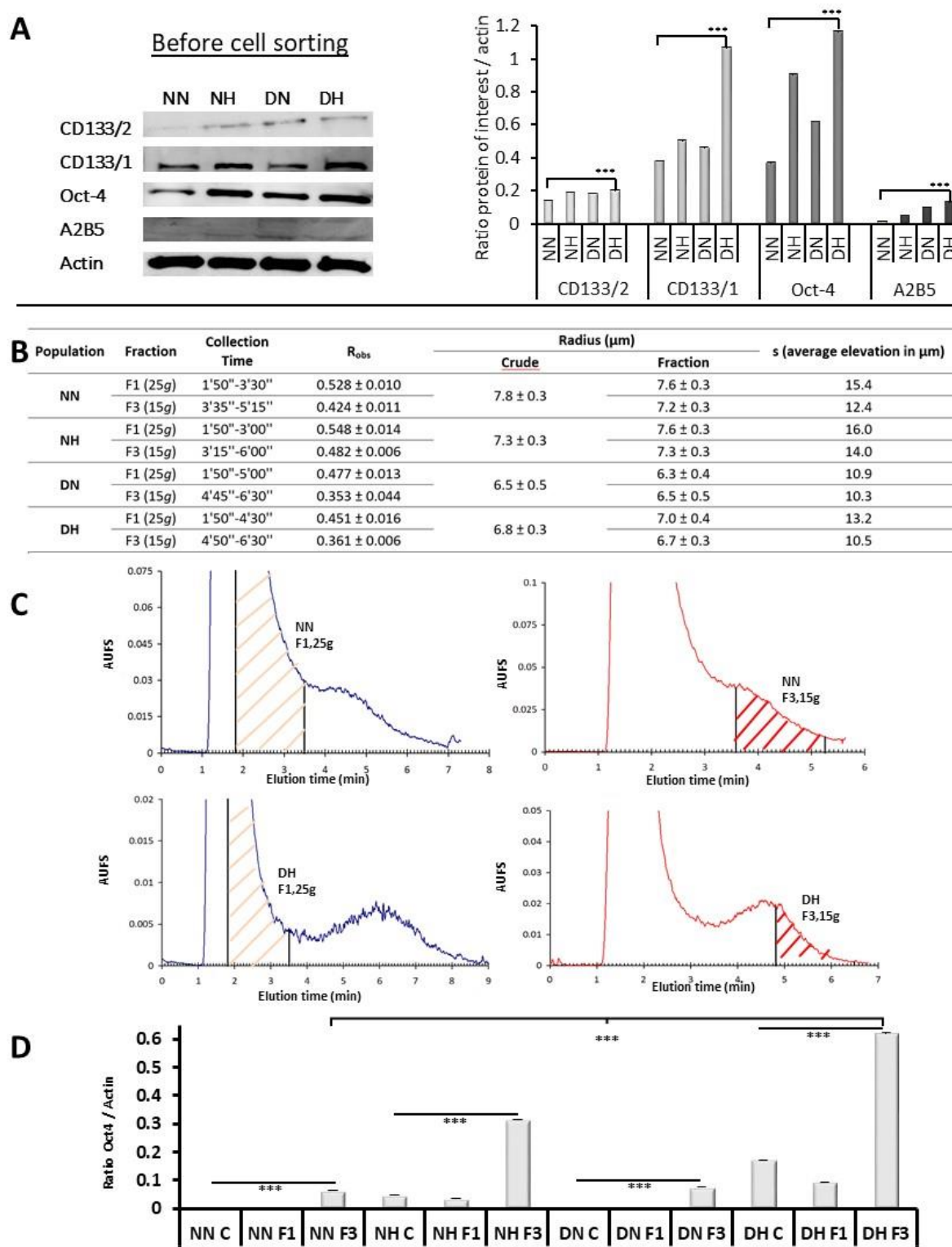


Figure 2. Production of cell subpopulations with increasing degrees of stemness. (A) CSC marker expression was evaluated in cells grown under four conditions (NN, NH, DN, and DH). Left panel, assessment of CD133/2, CD133/1, A2B5, and OCT-4 levels by western blotting. Actin was used as a loading control. Right panel, quantification of CSC marker expression, *** $p < 0.001$. (B) SdFFF elution conditions and results. The collection time, R_{obs} , radius, and s for fractions F1 and F3 of the four populations (NN, NH, DN, and DH) are shown. (C)

Representative SdFFF fractograms in the NN and DH conditions, in which the CSC content was lowest and highest, respectively. **(D)** Western blotting of OCT-4 in control cells (C = unsorted cell suspension) and cell subpopulations sorted by SdFFF. Actin was used as a loading control and for quantification. *** $p < 0.001$.

Proof Version

Sorting of CSCs using SdFFF: comparison with a gold standard. To record the most specific EM signatures with our biosensors, the populations selected by the culture conditions were further sorted to enrich cell populations based on their differentiation status. To this end, we used both the conventional magnetic separation method (gold standard) and SdFFF.

Magnetic sorting using CD133 beads (conventional method). CD133/1-coated magnetic beads were produced as described in the Supporting Information. Following magnetic cell sorting, expression of OCT-4 was measured by western blotting (Figure SI-1). OCT-4 expression differed before and after sorting (Figure 2A). Indeed, OCT-4 was still significantly higher in DH than in NN (1.6-fold; $p < 0.001$); however, in the previous experiment, the fold change in OCT-4 was 3.1 (Figure 2A). This result indicated that magnetic cell sorting did not successfully enrich for CSCs, or at least did not isolate cell subpopulations with distinct CSC contents.

SdFFF sorting. The usually described SdFFF elution mode for cells is the biocompatible “hyperlayer” mode^{26, 27, 40, 41}, in which subpopulations of cells are focused into a thin layer at an equilibrium position in the channel thickness, depending on their biophysical properties: size and density as first-order parameters, along with shape and rigidity²⁵. Hyperlayer elution order is size- and density- dependent: larger and less dense cells are focused in the faster streamlines, and are consequently eluted first. The experimental retention ratio, R_{obs} (void time divided by retention time [t_0 / t_R], measured by the first moment method)⁴², was calculated to determine the average velocities and elution modes (Figure 2B).

Under our elution conditions (0.8 mL/min; 15 or 25 g), we obtained similar fractograms with two major peaks, the first corresponding to non-retained species (void volume peak, $R_{\text{obs}} \approx 1$) and differentiated cells, and the second corresponding specifically to other cell subpopulations with $R_{\text{obs}} < 1$ (Figure 2C).

Hyperlayer elution mode was first determined based on the field and flow rate dependence of R_{obs} ^{40, 41}. Then, at equivalent flow rates, the increase in field strength focused cells in slower stream lines, increasing retention and decreasing R_{obs} ; this was observed for all conditions (Figure 2B). Except in the DN condition, we observed a decrease in cell radius from F1 to F3 within the same population, corresponding to elution based on size (Figure 2B). The size increase for DN may correspond to a significant density increase⁴³. The average density of the crude U87-MG cell population ranged from 1.058 to 1.064 (Table SI-1). Finally, in hyperlayer elution mode, samples were lifted away from the accumulation wall, limiting harmful cell–surface interactions. By using the following equation⁴⁴

$$s = \frac{R_{obs} \times \omega}{6}$$

in which ω is the channel thickness (175 μm), we calculated the value of s , the average distance from the center of the cell to the channel wall⁴⁴, which should be greater than the particle radius r , calculated from the mean cell diameter (Figure 2B).

U87-MG is a polydisperse population in terms of both biophysical properties (size and density, Figure 2B) and differentiation status. In a previous study⁴⁵, differentiated cells eluted in F1, whereas CSCs, which are smaller and denser, eluted in F3^{46, 47}. In this study, we eluted and collected cells under two fields to obtain an enriched population with a given differentiation status (Figure 2B). The 25 g external field strength improved retention of differentiated cells and their collection in F1 (Figure 2C, left panel), whereas the 15 g external field strength decreased cell retention, resulting in more gentle elution of stem cells in F3 (Figure 2C, right panel). As shown in Figure 2C, an important change in elution profile was observed between the NN and DH conditions, with more resolved peaks and decreased R_{obs} . These variations correlated with the increased proportions of CSCs from NN to DH conditions (Figure 2A).

To determine the sorting efficiency of CSCs using SdFFF, we measured the changes in OCT-4 expression in different subpopulations using western blotting (Figure 2D). Whatever the culture conditions (NN to DH), OCT-4 expression was significantly higher in the F3-derived subpopulation than in the overall population ($p < 0.001$) (Figure 2D). Furthermore, we observed a significant 7.6-fold increase in OCT-4 expression between NN F3 and DH F3 ($p < 0.001$). Based on OCT-4 expression, SdFFF achieved better CSC enrichment than magnetic cell sorting between NN and DH (9.7-fold vs. 1.6-fold), and was therefore suitable for the subsequent experiments. SdFFF enabled us to prepare eight subpopulations, from F1 NN to F3 DH, each of which had to be characterized phenotypically and functionally to determine their degree of differentiation.

Phenotypical characterization. Validation of the SdFFF method and phenotypical characterization of the isolated subpopulations were achieved by a proteome array that assesses the levels of 15 stem cell markers (Figure SI-2). The expression changes in these 15 proteins (Figure SI-2) were similar to those of OCT-4 (Figure 2D), regardless of culture and cell sorting conditions, confirming previously obtained results. Even though each protein tested had its own specific expression profile, the expression pattern of OCT-4 was representative of all 15 proteins tested (Figure S1-2 and SI-3). All proteins analyzed by the proteome arrays were more highly expressed ($p < 0.001$) in F3 fractions than in basal non-sorted conditions (NN, NH, DN, DH). The maximum fold change between basal and F3 conditions was observed in DH (Figure S1-2 and SI-2). The same experiment revealed that expression of 15 CSC-related proteins was significantly higher in DH F3 cells than in NN F3 cells ($p < 0.001$). This confirmed that SdFFF efficiently sorted CSCs, as it can be notably observed between the extreme conditions: NN to DH F3.

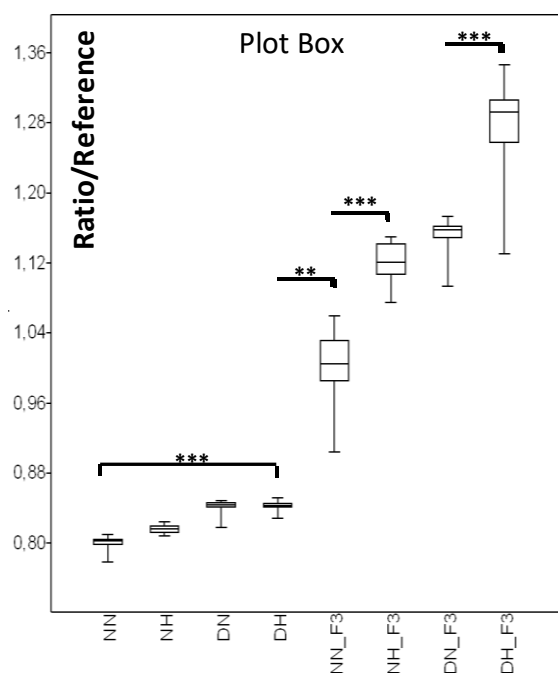


Figure 3. Quantification of protein expression under distinct culture conditions and following cell sorting using SdFFF. Expression of human pluripotent stem cell-related proteins was evaluated by a proteome array (see SI-1 and Figure SI-2). Expression of all proteins in a specific condition is showed in the box plot. An ANOVA was used to compare the different conditions. $p < 0.05$ was considered significant (** $p < 0.01$; *** $p < 0.001$).

Figure 3 shows a box plot depicting the differential expression of these 15 markers. First, the box plot distinguishes two different groups: the first includes all culture conditions without SdFFF cell sorting, whereas the second one (with a larger proportion of CSCs) includes the SdFFF sorting conditions. Two main effects can be observed from the box plot analysis: the first is due to the culture conditions, whereas the second is closely linked to cell sorting. The differences in the ratio between DH and NN and between DH and DH F3 were significant (both $p < 0.001$). Hypoxia and defined medium had an additive effect. The differences in the ratios between NN F3 and NH F3 sorting conditions and between DN F3 and DH F3 sorting conditions were significant ($p < 0.001$).

Altogether, these data demonstrate that a combination of defined culture conditions and cell sorting by SdFFF are required to optimize isolation of CSCs.

Functional characterization. Functional tests were performed to demonstrate two important properties of CSC: 1) self-renewal, which is the ability to give rise to differentiated progeny or colonies (*i.e.*, clonogenicity); 2) and quiescence (long cell cycle), which reduces proliferation⁴⁸. We measured the proliferation rate by performing BrdU incorporation in cells derived from SdFFF fractions F1 to F3 (Figure 4A). The F3/F1 proliferation ratio decreased between NN (0.49-fold) and DH conditions, reaching a minimum value in DH (0.09-fold). These data are convenient with the highly significant diminution of the proliferation rate previously observed in F3-derived cells irrespective of the conditions employed⁴⁵. The proliferation rate was reduced in the F3 cell population; therefore, we compared the clonogenic capacity of these cells and those in the F1 population. Clonogenicity assays on Matrigel revealed an increase in the area of colonies generated by cells derived from F1 and F3 (Figure 4B). The F3/F1 ratio increased between the NN and DH conditions, reaching a maximum (29.1-fold) in DH. Both BrdU

incorporation and the clonogenicity assay demonstrated that F3-derived cells had an increased CSC content.

Proof Version

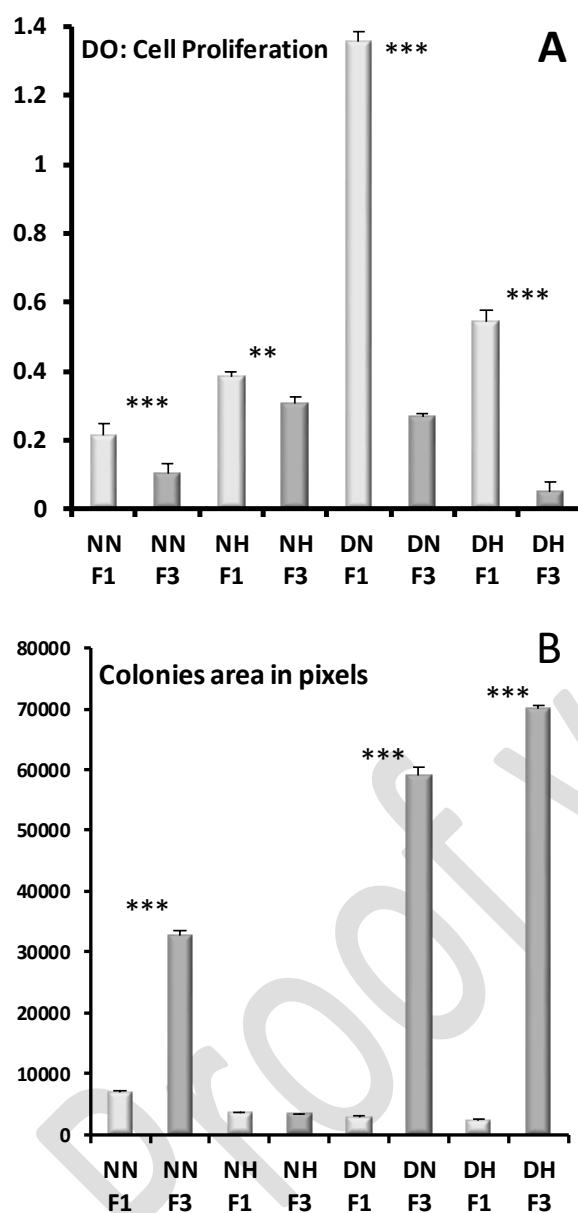


Figure 4. Functional tests after cell sorting with SdFFF. (A) Cell proliferation was evaluated by BrdU incorporation and measurement of optical density at 540 nm. (B) Clonogenicity was evaluated on Matrigel and colony size was evaluated by measuring the pixel area.

Obtainment of specific EM signatures

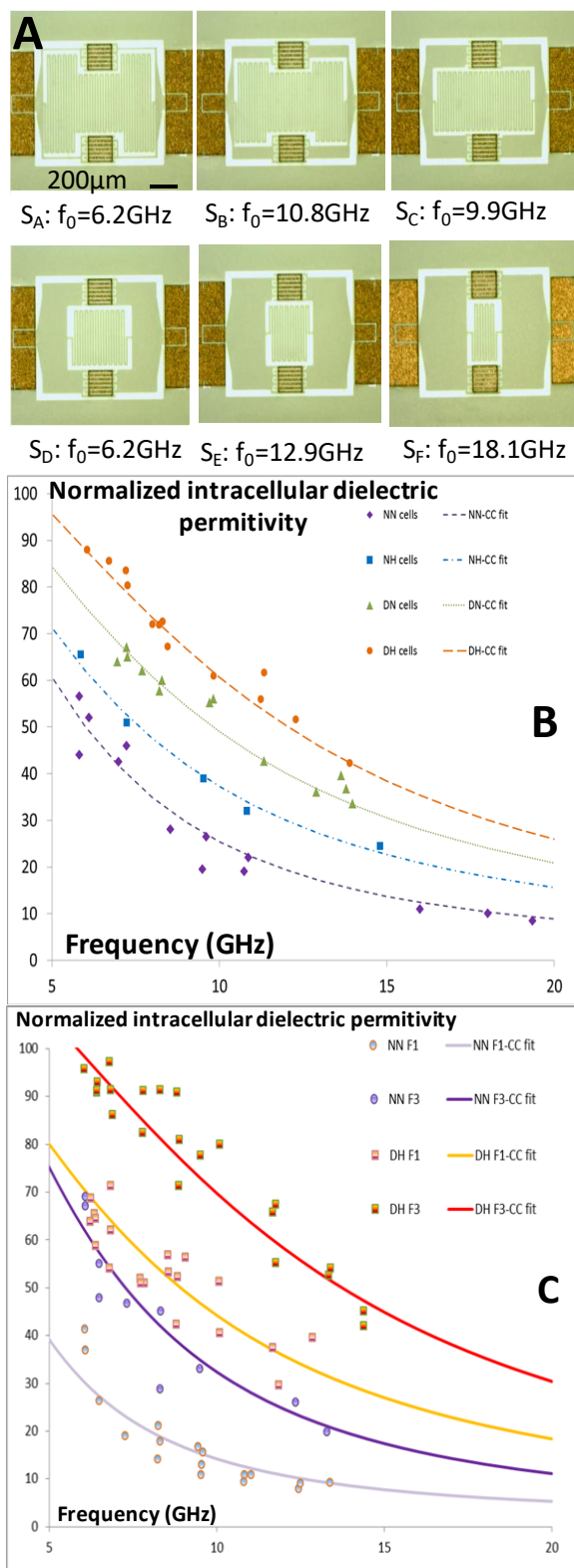
Our method is based on characterization of intracellular content based on dielectric properties, using the microwave biosensors presented in Materials and Methods. This approach allowed us to perform microwave spectroscopy analysis on different cell subpopulations. In practice, we used different biosensor designs, as illustrated in Figure 5A. In fact, 10 biosensors were designed to allow characterization on a wide frequency band in order to establish a significant EM signature. Hence, the six biosensors presented in Figure 5A operated at 6.2, 7.5, 9.9, 10.8, 12.9 and 18.1 GHz.

From the data collected at all investigated frequencies, an average EM signature was plotted for each cell population (Figure 5B and C). The raw data follow the frequency dependence of the relative permittivity of intracellular content. A physical model was introduced and applied to fit the data and establish an average signature based on a Cole–Cole equation (2), conventionally used to describe dispersion phenomenon and frequency dependence in biological media⁴⁹.

To link biological and physical parameters, the intracellular content of a cell must be examined. Another biological parameter that is often used to assess the presence of CSCs is the N:C ratio (i.e., the ratio of cytoplasmic to nuclear volumes) because CSCs have relatively large nuclei. The decrease in this ratio between NN and DH conditions was not significant (Figure SI-4), but the value reached a minimum (~2.8-fold) under DH conditions, which corresponded to an increased CSC content in DH *vs.* NN. Cell contents influence conductivity and permittivity, which are physical parameters.

Figure 5B shows the resulting EM signatures corresponding to basal conditions (NN, NH, DN, and DH). As expected, the dielectric permittivity of cell contents exhibits dispersive behavior

Proof Version



C) EM signatures before and after cell sorting. These signatures were obtained using the protocol and mathematical model described in the Materials and Methods section. The model parameters are provided in Table SI-2.

Figure 5. Obtainment of specific EM signatures. (A) Biosensor design. (B and

when frequency increases, with maximum discrimination in the lower part of the investigated frequency band, between 5 and 10 GHz, where most of the relaxation of water molecules actually occurs. The intrinsic intracellular dielectric permittivity increased between NN and DH. This effect was due to biological differences between cultured cells, as reflected by comparison of the N:C ratio (Figure SI-4).

Nevertheless, superpositions could be observed without cell sorting. To achieve a higher degree of discrimination and establish the best individualized EM signatures, SdFFF cell sorting was of prime importance, as illustrated in Figure 5C. The most differentiated cells (F1 cell fraction) had a less intracellular dielectric permittivity, according to the increase in the frequency parameter, than cells in F3 (most undifferentiated cells); this difference persisted irrespective of culture conditions. The largest difference in EM signature was observed between NN F1 and DH F3, which respectively had the lowest and highest proportions of CSCs. In fact, the EM signatures corresponding to NN F3 and DH F1 had some overlap, whereas signatures corresponding to NN F3 and DH F3 were significantly individualized, as were those corresponding to NN F1 and DH F3 ($p < 0.001$). This physical parameter permits recognition of cell types, and is superior to previously reported parameters. Thus, we obtained a unique signature that permits us to recognize CSCs.

Each biological parameter corresponds to a physical parameter, including SdFFF, for which the sorting conditions represent an independent, unique, and specific EM signature.

The link between physical and biological parameters can be explained in terms of the measured intracellular permittivity and its inverse relationship with conductivity. The best example is in the DH condition, in which the nuclear volume was significantly higher than the

cytoplasmic volume, implying a decrease of ionic conductivity, resulting in a global increase in the intracellular permittivity.

Conclusion.

All the parameters used in this study demonstrated the presence of CSCs and a unique EM signature for the different cell populations. The gradual enrichment in CSCs permitted the construction of a large panel of subpopulations with a low proportion of CSCs under NN conditions and a large proportion under DH conditions. The results demonstrate that microwave dielectric spectroscopy, a radically new approach, is an effective way to distinguish stem cells. The specific EM signatures that we identified represent innovative biomarkers that are expected to be complementary to conventional methods, especially given their potential for analyzing intracellular content in a non-invasive manner. The next step in development of this technique will be the investigation of living cells in their biological environment. In these future efforts, the main challenge will be to maintain the same sensitivity achieved in this study, in which the cells were measured in air. For this purpose, microfluidic technologies represent the optimal approach, as they allow the researcher to mimic the cellular environment and minimize the analytical volume, thereby limiting the impact of biological media losses on biosensor performance. In light of the hyphenation of asymmetrical flow FFF and MALS for characterization of nano-sized species, this study should also be considered a first step to develop a new SdFFF detector dedicated to cell sorting and characterization. This approach, in an integrated microfluidic solution, should be an effective label-free method to sort stem cells after establishing a selective EM databank. Moreover, the databank could be enlarged by using

this method *in vivo* on human glioblastomas or for other types of tumors (*e.g.*, colorectal cancer, CRC) for which tissues are easier to collect.

In conclusion, the new instrumental and methodological approaches developed in this study should enhance the evaluation of CSCs in tumors, opening the door to novel therapeutic uses. The unique and specific signature of CSCs that we identified should facilitate the development of new diagnostic, prognostic, and theranostic applications.

Acknowledgments

This study was supported by Région Limousin, FEDER, the European project SUMCASTEC (Horizon 2020 research and innovation programme under grant agreement No 737164), and Ligues contre le cancer Régionales (Haute Vienne, Creuse et Corrèze).

Competing Interests

The authors declare that no competing interest exists.

References

- Ohgaki, H.; Dessen, P.; Jourde, B.; Horstmann, S.; Nishikawa, T.; Di Patre, P. L.; Burkhard, C.; Schuler, D.; Probst-Hensch, N. M.; Maiorka, P. C.; Baeza, N.; Pisani, P.; Yonekawa, Y.; Yasargil, M. G.; Lutolf, U. M.; Kleihues, P., *Cancer Res.* **2004**, *64* (19), 6892-6899.
- Chen, J.; McKay, R. M.; Parada, L. F., *Cell* **2012**, *149* (1), 36-47.
- Reardon, D. A.; Rich, J. N.; Friedman, H. S.; Bigner, D. D., *J. Clin. Oncol.* **2006**, *24* (8), 1253-1265.
- Lathia, J. D.; Mack, S. C.; Mulkearns-Hubert, E. E.; Valentim, C. L. L.; Rich, J. N., *Genes & Development* **2015**, *29* (12), 1203-1217.
- Reya, T.; Morrison, S. J.; Clarke, M. F.; Weissman, I. L., *Nature* **2001**, *414* (6859), 105-111.
- Singh, S. K.; Clarke, I. D.; Terasaki, M.; Bonn, V. E.; Hawkins, C.; Squire, J.; Dirks, P. B., *Cancer Res.* **2003**, *63* (18), 5821-5828.
- Visvader, J. E.; Lindeman, G. J., *Nat. Rev. Cancer* **2008**, *8* (10), 755-768.
- Bao, S. D.; Wu, Q. L.; McLendon, R. E.; Hao, Y. L.; Shi, Q.; Hjelmeland, A. B.; Dewhirst, M. W.; Bigner, D. D.; Rich, J. N., *Nature* **2006**, *444* (7120), 756-760.
- Cheng, L.; Wu Q Fau - Huang, Z.; Huang Z Fau - Guryanova, O. A.; Guryanova Oa Fau - Huang, Q.; Huang Q Fau - Shou, W.; Shou W Fau - Rich, J. N.; Rich Jn Fau - Bao, S.; Bao, S., *EMBO J.* **2011**, *30*, 800-813.
- Beier, D.; Schulz, J. B.; Beier, C. P., *Mol Cancer* **2011**, *10*, 128.
- Islam, F.; Gopalan, V.; Smith, R. A.; Lam, A. K. Y., *Experimental Cell Research* **2015**, *335* (1), 135-147.
- Mathonnet, M.; Perraud, A.; Christou, N.; Akil, H.; Melin, C.; Battu, S.; Jauberteau, M. O.; Denizot, Y., *World J. Gastroenterol.* **2014**, *20* (15), 4189-4196.
- Vassilopoulos, A.; Wang, R. H.; Petrovas, C.; Ambrozak, D.; Koup, R.; Deng, C. X., *Int. J. Biol. Sci.* **2008**, *4* (3), 133-142.
- Vermeulen, L.; Todaro, M.; Mello, F. D.; Sprick, M. R.; Kemper, K.; Alea, M. P.; Richel, D. J.; Stassi, G.; Medema, J. P., *Proc. Natl. Acad. Sci. U. S. A.* **2008**, *105* (36), 13427-13432.
- Ponti, D.; Costa, A.; Zaffaroni, N.; Pratesi, G.; Petrangolini, G.; Coradini, D.; Pilotti, S.; Pierotti, M. A.; Daidone, M. G., *Cancer Res.* **2005**, *65* (13), 5506-5511.
- O'Brien, C. A.; Pollett, A.; Gallinger, S.; Dick, J. E., *Nature* **2007**, *445* (7123), 106-110.
- Ricci-Vitiani, L.; Lombardi, D. G.; Pilozzi, E.; Biffoni, M.; Todaro, M.; Peschle, C.; De Maria, R., *Nature* **2007**, *445* (7123), 111-115.
- Charafe-Jauffret, E.; Ginestier, C.; Iovino, F.; Wicinski, J.; Cervera, N.; Finetti, P.; Hur, M. H.; Diebel, M. E.; Monville, F.; Dutcher, J.; Brown, M.; Viens, P.; Xerri, L.; Bertucci, F.; Stassi, G.; Dontu, G.; Birnbaum, D.; Wicha, M. S., *Cancer Res.* **2009**, *69* (4), 1302-1313.
- Ginestier, C.; Hur, M. H.; Charafe-Jauffret, E.; Monville, F.; Dutcher, J.; Brown, M.; Jacquemier, J.; Viens, P.; Kleer, C. G.; Liu, S. L.; Schott, A.; Hayes, D.; Birnbaum, D.; Wicha, M. S.; Dontu, G., *Cell Stem Cell* **2007**, *1* (5), 555-567.
- Ho, M. M.; Ng, A. V.; Lam, S.; Hung, J. Y., *Cancer Res.* **2007**, *67* (10), 4827-4833.
- Yin, A. H.; Miraglia, S.; Zanjani, E. D.; Almeida-Porada, G.; Ogawa, M.; Leary, A. G.; Olweus, J.; Kearney, J.; Buck, D. W., *Blood* **1997**, *90* (12), 5002-5012.
- Bidlingmaier, S.; Zhu, X. D.; Liu, B., *J. Mol. Med.* **2008**, *86* (9), 1025-1032.
- Kemper, K.; Sprick, M. R.; de Bree, M.; Scopelliti, A.; Vermeulen, L.; Hoek, M.; Zeilstra, J.; Pals, S. T.; Mehmet, H.; Stassi, G.; Medema, J. P., *Cancer Res.* **2010**, *70* (2), 719-729.
- Yakisich, J. S.; Azad, N.; Kaushik, V.; Iyer, A. K. V., *J Cell Physiol* **2017**, *232* (9), 2280-2286.

25. Faye, P. A.; Vedrenne, N.; De la Cruz-Morcillo, M. A.; Barrot, C. C.; Richard, L.; Bourthoumieu, S.; Sturtz, F.; Funalot, B.; Lia, A. S.; Battu, S., *Anal. Chem.* **2016**, *88* (13), 6696-6702.
26. Naves, T.; Battu, S.; Jauberteau, M.-O.; Cardot, P. J. P.; Ratinaud, M.-H.; Verdier, M., *Anal. Chem.* **2012**, *84* (Copyright (C) 2012 American Chemical Society (ACS). All Rights Reserved.), 8748-8755.
27. Mélin, C.; Perraud, A.; Akil, H.; Jauberteau, M. O.; Cardot, P.; Mathonnet, M.; Battu, S., *Anal. Chem.* **2012**, *84* (3), 1549-1556.
28. Artis, F.; Chen, T.; Chretiennot, T.; Fournie, J. J.; Poupot, M.; Dubuc, D.; Grenier, K., *IEEE Microw. Mag.* **2015**, *16* (4), 87-96.
29. Yang, Y.; Zhang, H. Q.; Zhu, J. J.; Wang, G. Y.; Tzeng, T. R.; Xuan, X. C.; Huang, K. M.; Wang, P. S., *Lab Chip* **2010**, *10* (5), 553-555.
30. Bryan, A. K.; Hecht, V. C.; Shen, W.; Payer, K.; Grover, W. H.; Manalis, S. R., *Lab Chip* **2014**, *14* (3), 569-576.
31. Salimi, E.; Braasch, K.; Butler, M.; Thomson, D. J.; Bridges, G. E., *Biomicrofluidics* **2016**, *10* (1), 014111.
32. Dalmay, C.; Cheray, M.; Pothier, A.; Lalloue, F.; Jauberteau, M. O.; Blondy, P., *Sens. Actuator A-Phys.* **2010**, *162* (2), 189-197.
33. Williams, S. K. R.; Runyon, J. R.; Ashames, A. A., *Anal. Chem. (Washington, DC, U. S.)* **2011**, *83* (Copyright (C) 2011 American Chemical Society (ACS). All Rights Reserved.), 634-642.
34. Bertrand, J.; Liagre, B.; Bégaud-Grimaud, G.; Jauberteau, M. O.; Cardot, P.; Beneytout, J. L.; Battu, S., *J. Chromatogr. B* **2008**, *869*, 75-78.
35. Battu, S.; Elyaman, W.; Hugon, J.; Cardot, P. J. P., *Biochim. Biophys. Acta* **2001**, *1528* (2-3), 89-96.
36. Battu, S.; Cook-Moreau, J.; Cardot, P. J. P., *J. Liq. Chromatogr. Relat. Technol.* **2002**, *25* (13 - 15), 2193-2210.
37. Bégaud-Grimaud, G.; Battu, S.; Liagre, B.; Beneytout, J. L.; Jauberteau, M. O.; Cardot, P. J. P., *J. Chromatogr. A* **2009**, *1216* (52), 9125-9133.
38. Zhang, L. Y.; du Puch, C. B. M.; Dalmay, C.; Lacroix, A.; Landoulsi, A.; Leroy, J.; Melin, C.; Lalloue, F.; Battu, S.; Lautrette, C.; Giraud, S.; Bessaudou, A.; Blondy, P.; Jauberteau, M. O.; Pothier, A., *Sens. Actuator A-Phys.* **2014**, *216*, 405-416.
39. Bao, B.; Ahmad, A.; Azmi, A. S.; Ali, S.; Sarkar, F. H., *Curr Protoc Pharmacol* **2013**, Chapter 14, Unit 14 25.
40. Bégaud-Grimaud, G.; Battu, S.; Leger, D. Y.; Cardot, P. J. P., Mammalian Cell Sorting with Sedimentation Field Flow Fractionation. In *Field-Flow Fractionation in Biopolymer Analysis*, Williams, S. K. R.; Caldwell, K. D., Eds. Springer-Verlag: Wien, 2012.
41. Caldwell, K. D., Steric field-flow fractionation and steric transition. In *Field-flow fractionation handbook*, Schimpf, M. E.; Caldwell, K. D.; Giddings, J. C., Eds. John Wiley & Sons, Inc.: New York, 2000; pp 79-94.
42. Williams, P. S.; Lee, S.; Giddings, J. C., *Chem. Eng. Commun.* **1994**, *130*, 143-166.
43. Leger, D. Y.; Battu, S.; Liagre, B.; Cardot, P. J. P.; Beneytout, J. L., *J. Chromatogr. A* **2007**, *1157* (1-2), 309-320.
44. Chmelik, J., *J. Chromatogr. A* **1999**, *845* (1-2), 285-291.
45. Bertrand, J.; Bégaud-Grimaud, G.; Bessette, B.; Verdier, M.; Battu, S.; Jauberteau, M. O., *Int. J. Oncol.* **2009**, *34*, 717-727.
46. Huang, X.; Ketova, T.; Litington, Y.; Chiang, C., *J Vis Exp* **2010**, (43), pii: 2086.
47. Zhao, Y.; Huang, Q.; Zhang, T.; Dong, J.; Wang, A.; Lan, Q.; Gu, X.; Qin, Z., *Ultrastruct Pathol* **2008**, *32* (6), 241-5.

48. Boman, B. M.; Wicha, M. S., *J. Clin. Oncol.* **2008**, 26 (17), 2795-2799.
49. Markx, G. H.; Davey, C. L., *Enzyme Microb. Technol.* **1999**, 25 (3-5), 161-171.

Proof Version

Abstract Graphic:

